

Transactions, SMiRT-27
Yokohama, Japan, March 3-8, 2024
Division III

ANALYTICAL STUDY ON BEHAVIOR OF RC PANELS COVERED WITH STEEL PLATE IMPACTED BY VARIED MISSILE WEIGHT

Ryosuke Imai¹, Takaaki Tsukada², Shin Kuramoto², and Yasuhiro Ohashi²

¹ Nuclear Projects Division, Shimizu Corporation, Kyobashi Chuo-ku, Tokyo, JAPAN
(r_imai@shimz.co.jp)

² Nuclear Projects Division, Shimizu Corporation, Kyobashi Chuo-ku, Tokyo, JAPAN

ABSTRACT

The installation of a steel plate on the rear surface of the reinforced concrete (RC), herein referred to as half steel concrete (HSC), is anticipated to effectively prevent missiles from perforating the wall. Additionally, the steel plate prevents the dispersion of crushed concrete inside the buildings due to missile impact. However, these local damage criteria formulas have not been developed or applied in aircraft impact design.

Experimental research was undertaken to assess the impact resistance performance of HSCs [Hashimoto et al. (2005)], and the effectiveness of enhanced impact resistance was verified. In the prior study, the formula for the local damage criteria intended for the design of HSC was proposed, based on impact test results in which the critical bulging height of the steel plate was determined to be 53.8mm.

Given the enhanced computational capability of FEM analysis, a precise simulation of the ultimate behaviour of HSCs has become feasible. Energy absorption mechanisms within the crushed concrete and the deformation of the steel plate were investigated by simulating the results of impact tests [T. Tsukada (2022)]. However, the impact parameters in prior experimental and analytical investigations were limited to impact velocity, panel thickness, and steel plate thickness. Recognizing the missile weight and concrete strength as important factors in formulating the local damage criteria of HSC, this study delves into additional analytical research aimed at investigating the influence of missile weight and concrete strength on the local damage criteria of HSC.

INTRODUCTION

The design of nuclear-related facilities, to withstand extreme conditions like accidental aircraft impact or unforeseen terrorist attacks, holds vital societal significance. In the context of these facilities, reinforced concrete panels are commonly used. Numerous studies have been conducted to evaluate the resistance of these reinforced concrete panels to missile impacts. In terms of localized damage to reinforced concrete panels, various formulas have been proposed to determine the necessary thickness of these panel to prevent perforation or scabbing on their rear surface [W. S. Chang (1981), NDRC (1946), P. Degen (1980)].

The HSC system is anticipated to offer effectiveness in preventing missiles from penetrating walls and containing the dispersion of crushed concrete. Consequently, adopting HSC provides a strong possibility for optimizing wall or roof thickness against missile impact. This optimization directly correlates with material consumption and construction costs. However, these formulas for local damage criteria have not been developed or implemented in the aircraft impact design involving HSCs. The formula proposed in this study offers structural designers a cost-effective means to assess wall impact resistance, complementing traditional FEM analysis. Particularly advantageous in the early design phases, this formula allows for the determination of wall thickness before committing to more in-depth studies, providing a practical and efficient tool for preliminary evaluations.

Experimental research was conducted to assess the impact resistance performance of HSCs, as outlined in Figure 1 [Hashimoto et al. (2005)]. The effectiveness of enhanced impact resistance was verified. In the previous study, a formula was proposed to establish the local damage criteria for HSC design. This

formula based on the results of impact tests that identified a critical bulging height of the steel plate at 53.8mm. However, this critical bulging height of 53.8mm was derived from the impact test case that resulted in failure through the splitting mode. This occurred when the HSC panel, consisting of 80mm thick concrete overlaid with a 0.8mm thick steel plate, was subjected to a high-velocity impact from a hard missile with an impact weight of $M_{m0} = 0.486\text{kg}$ and an impact velocity of $V_m = 250\text{m/s}$. In this scenario, the occurrence of a small crack on the steel plate located at the rear face was identified as reaching a critical state.

To establish a comprehensive design formula to prevent local failures in HSCs, it is necessary to attain a more universal representation of the critical state. An analytical investigation using the impact analysis model shown in Figure 2 was undertaken by Tsukada et al. (2022). This involved simulations of various impact test results, as conducted by Hashimoto et al. (8 impact tests for RCs and 16 for HSCs). Table 1 summarises the comparison of failure modes between experimental and analytical results in Tsukada et al. (2022) to verify the modelling of RC and HSC panels. The analysis results show good agreement with the experimental results. The comparisons of typical failure modes of HSCs between impact tests and analysis are shown in Table 2. This study aimed to explore the energy absorption mechanisms within crushed concrete and the deformation of the steel plate. The results of the analytical study revealed a significant correlation between the absorbed energy of concrete, E_c , and the impact velocity V_m as shown in Figure 3. This V_m influences the pressure exerted on the concrete and enhances the concrete's strength through the strain rate effect. Tsukada et al. (2022) presented a prospective approach wherein the energy required by the steel plate to prevent perforation can be assessed through a comparison involving the difference between the residual kinematic energy of the missile and the E_c against the energy absorption capability of the steel plates, E_s .

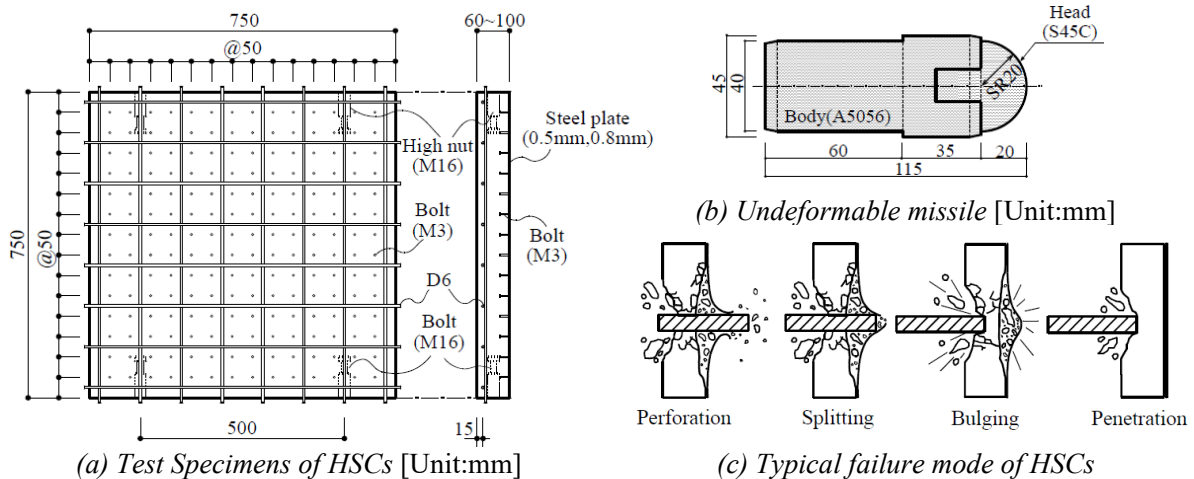


Figure 1. Test specimens and typical failure modes in impact test for HSCs [Hashimoto et al. (2005)]

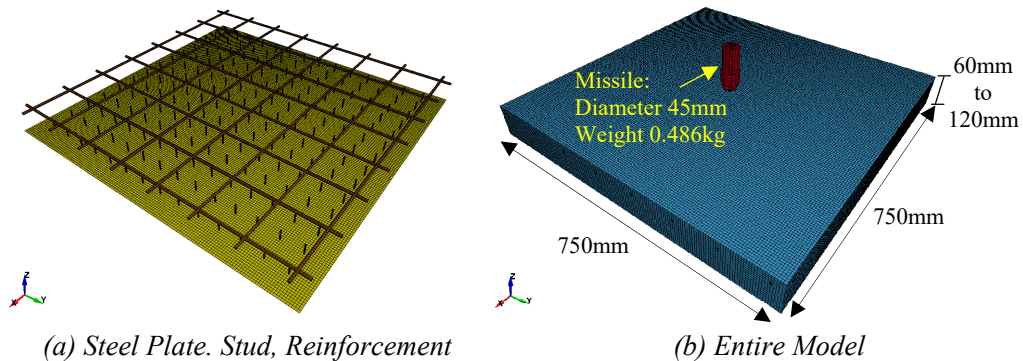


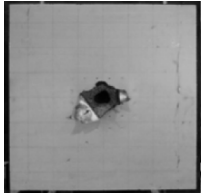
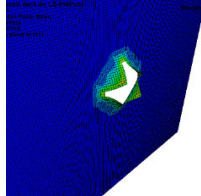
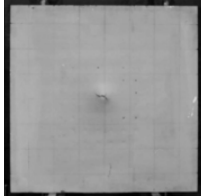
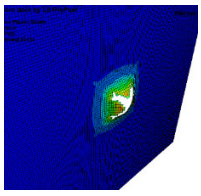
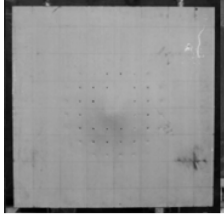
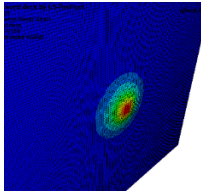
Figure 2. Impact analysis model

Table 1: Comparison of failure mode between experimental and analytical results


Test/ Analysis Case		Impact Test				Impact Analysis			
		Test Parameter			Failure Mode	Failure Mode*1	Initial Kinematic Energy of Missile K_m (J)	Absorbed Energy (J)	
		Panel Thickness t (mm)	Steel Plate Thickness T (mm)	Target Velocity V_m (m/sec)				Concrete E_c	Steel Plate E_s
No.	Label								
T1	RC-N-1	60	/	175	Perforation	Perforation	7446	6844	/
T2	RC-N-2	80		175	Perforation	Perforation	7446	7169	
T3	RC-N-3	100		175	Scabbing	Scabbing	7446	7096	
T4	RC-N-4	100		215	Perforation	Perforation	11240	10771	
T5	RC-N-5	100		215	Perforation	Perforation	11240	10762	
T6	RC-N-6	120		215	Scabbing	Scabbing	11240	10607	
T7	RC-N-7	120		250	Perforation	Perforation	15200	14443	
T8	RC-N-8	150		250	Penetration	Scabbing	15200	14286	
T9	HSC-N-1	60	0.5	140	Splitting	Splitting	4766	4445	184
T10	HSC-N-2	80		140	Bulging	Bulging	4766	4511	129
T11	HSC-N-3	60		175	Perforation	Perforation	7446	6786	225
T12	HSC-N-4	80		175	Bulging	Bulging	7446	6993	241
T13	HSC-N-5	80		215	Perforation	Perforation	11240	10589	260
T14	HSC-N-6	100		250	Bulging	Bulging	15200	14451	307
T15	HSC-N-7	60		0.8	175	Bulging	Perforation	7446	6755
T16	HSC-N-8	60	175		Bulging	Perforation	7446	6759	318
T17	HSC-N-9	80	175		Bulging	Bulging	7446	6963	280
T18	HSC-N-10	60	215		Perforation	Perforation	11240	9932	381
T19	HSC-N-11	80	215		Bulging	Bulging	11240	10568	404
T20	HSC-N-12	80	250		Perforation	Perforation	15200	14158	432
T21	HSC-N-13	100	250		Bulging	Bulging	15200	14380	361
T22	HSC-N-14	80	1.2	175	Bulging	Bulging	7446	6973	258
T23	HSC-N-15	80		215	Bulging	Bulging	11240	10511	454
T24	HSC-N-16	80		250	Splitting	Splitting	15200	14132	589

Note *1: The different failure mode from test result is shaded. The reason of differences is described in Tsukada et al. (2022)

Table 2: Comparisons of typical failure mode of HSCs between experimental and analytical results [Tsukada et al. (2022)]

	Experimental Result (Rear Side)	Analysis Result		Experimental Result (Rear Side)	Analysis Result
Perforation	HSC-N-3		Splitting	HSC-N-16	
					
Bulging	HSC-N-11				
					

Effective Plastic Strain (%)



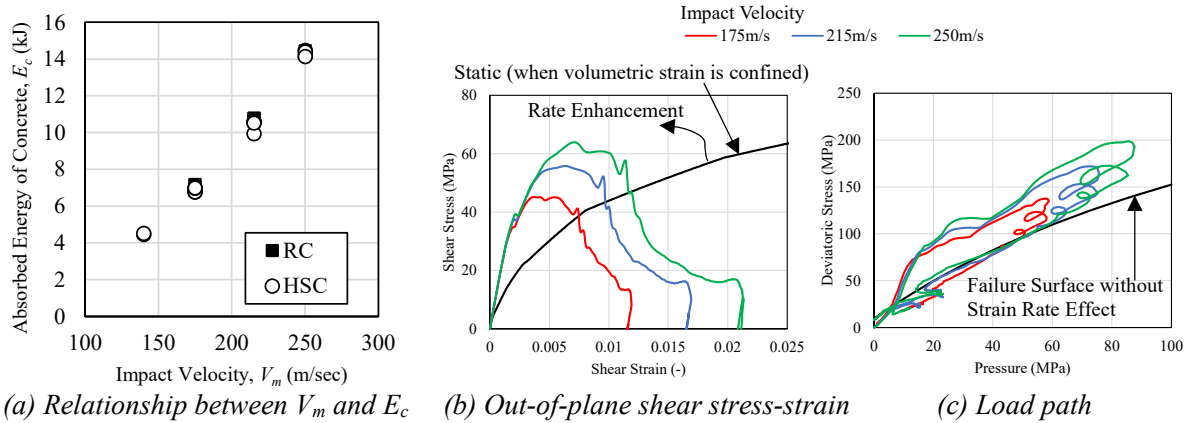


Figure 3. Relationship between V_m and E_c , and rate enhancement [Tsukada et al. (2022)]

The primary objective of this paper is to formulate and verify the local failure criteria for HSCs that cover a wide range of scenarios. The criteria are intended to have a general expression based on the unique energy absorption mechanisms of HSCs, making them applicable to various situation. To develop the local failure criteria of HSCs, it is essential to consider impact parameters that were not addressed in the impact test outlined in Table 1, such as the missile weight, M_m , and concrete strength, f_c' . Additionally, extrapolating V_m is necessary for criteria development. This paper conducts supplementary analyses outlined in Table 3 to comprehensively address the effect of M_m, f_c' and extrapolated V_m on the local failure criteria of HSC. Based on the outcomes, the proposed local failure criteria are presented, followed by verification analyses outlined in Table 4 to validate their effectiveness.

ANALYSIS CONDITIONS

The analysis models in the series of RCs and HSCs were all reinforced with deformed bars of 6.35mm diameter, spaced 100mm apart. In the HSCs series, 750mm square steel plates were fixed on the rear surface of RC panels using stud bolts, spaced 50mm apart. The compressive strength of the concrete used in this experiment is 30MPa. The RC and HSC panels were hanged in the air in the impact test.

The Concrete panel is modelled using solid elements to assess local damage due to the impact of a non-deformable missile. The steel plate installed on the rear surface of panel for HSCs is modelled using shell elements. The studs and reinforcements are modelled using bar elements. The nodes of steel panel, stud and reinforcement model are shared with those of the concrete model.

The Material model for concrete is the Karagozian & Case (K&C) concrete model which was verified in Crawford et al. (2011) and is already implemented in LS-DYNA. The shear failure surface is defined by the yield, maximum and residual failure surface, based on the relationship between volumetric strain and hydrostatic pressure. The softening of concrete in compression and tension is modelled based on the isotropic damage function which depends on the effective plastic strain. Dynamic increase factors are considered as a function of strain rate for compression, as per approach of the CEB Model Code (2013) and as per the modified CEB formulation proposed in Malvar et al. (1998).

The Material model for steel plates and reinforcements is chosen to be a piecewise linear plasticity model that allows the definition of an arbitrary stress versus strain curve. The properties of the steel plate and reinforcement considered in the analysis comply with the values obtained from impact tests. To demonstrate the fracture of steel plate, the element erosion criteria are considered according to their average elongation at fracture obtained from material testing with a triaxiality factor ($TF = 2$) for biaxial tension. The studs and missile are supposed as a linear elasticity model. Element erosion is considered only for steel plate when its strain reaches the elongation at fracture divided by TF. Element erosion for concrete is not considered because the concrete loses stiffness for bonding when it is damaged.

ANALYSIS CASE AND RESULTS

During the impact test for the RCs and HSCs, cases that exhibited a failure mode of perforation were not tested higher impact velocities. To establish a relationship between E_c and impact parameters, such as V_m , M_m and f_c' , supplementary analysis cases outlined in Table 3 were conducted in conjunction with the original impact test cases. It's important to note that the intentional setting of failure modes as perforation in most analysis cases is aimed at investigating the expected energy absorption mechanism when the HSC is perforated. This deliberate approach aligns with the specific objective of the analysis.

Table 3: Supplemental analysis results to establish relationship between impact parameters and E_c

Additional Analysis Case		Impact Parameters				Impact Analysis Results					
		Concrete Strength f_c' (MPa)	Missile Weight Multiplier M_m / M_{m0}	Panel Thickness t (mm)	Steel Plate Thickness T (mm)	Target Velocity V_m (m/sec)	Failure Mode	Initial Kinematic Energy of Missile K_m (J)	Absorbed Energy by Concrete E_c (J)		
No.	Label										
A1	RC100-V250-M1.0-Fc30	30	1.0	100	0.5	250	Perforation	15200	14556		
A2	RC120-V300-M1.0-Fc30			120		300	Perforation	21900	20918		
A3	RC120-V350-M1.0-Fc30			120		350	Perforation	29800	28530		
A4	RC120-V400-M1.0-Fc30			120		400	Perforation	38900	37237		
A5	HSC60-T0.5-V250-M1.0-Fc30			60	250	Perforation	15200	13160			
A6	HSC60-T0.5-V300-M1.0-Fc30			60	300	Perforation	21900	18462			
A7	HSC100-T0.5-V300-M1.0-Fc30			100	300	Perforation	21900	20782			
A8	HSC80-T0.8-V300-M1.0-Fc30			80	0.8	300	Perforation	21900	20167		
A9	HSC120-T0.5-V300-M1.0-Fc30	30	1.0	120	0.5	300	Bulging	21900	20836		
A10	HSC120-T0.5-V300-M1.2-Fc30		1.2				Bulging	26300	25019		
A11	HSC120-T0.5-V300-M1.5-Fc30		1.5				Perforation	32800	31227		
A12	HSC120-T0.5-V300-M2.0-Fc30		2.0				Perforation	43800	41123		
A13	HSC120-T0.5-V350-M1.0-Fc30		1.0			350	Bulging	29800	28441		
A14	HSC120-T0.5-V350-M1.2-Fc30		1.2				Perforation	35700	34030		
A15	HSC120-T0.5-V350-M1.5-Fc30		1.5				Perforation	44700	42279		
A16	HSC120-T0.5-V350-M2.0-Fc30		2.0				Perforation	59600	55340		
A17	HSC120-T0.5-V400-M1.0-Fc30		1.0			400	Perforation	38900	37122		
A18	HSC120-T0.5-V400-M1.2-Fc30		1.2				Perforation	46700	44350		
A19	HSC120-T0.5-V400-M1.5-Fc30		1.5				Perforation	58400	54897		
A20	HSC120-T0.5-V400-M2.0-Fc30		2.0				Perforation	77800	71376		
A21	HSC60-T0.5-V300-M1.0-Fc20	20	1.0	60	0.5	300	Bulging	21900	18232		
A22	HSC60-T0.5-V300-M1.0-Fc25	25					Perforation	21900	18239		
A23	HSC60-T0.5-V300-M1.0-Fc30	30					Perforation	21900	18298		
A24	HSC60-T0.5-V300-M1.0-Fc35	35					Perforation	21900	18405		
A25	HSC60-T0.5-V300-M1.0-Fc40	40					Perforation	21900	18534		
A26	HSC60-T0.5-V300-M1.0-Fc50	50					Perforation	21900	18802		
A27	HSC80-T0.5-V180-M1.0-Fc20	20				80	0.5	180	Bulging	7880	5220
A28	HSC80-T0.5-V180-M1.0-Fc25	25							Bulging	7880	5215
A29	HSC80-T0.5-V180-M1.0-Fc30	30							Bulging	7880	5207
A30	HSC80-T0.5-V180-M1.0-Fc35	35							Bulging	7880	5194
A31	HSC80-T0.5-V180-M1.0-Fc40	40	Bulging	7880	5184						
A32	HSC80-T0.5-V180-M1.0-Fc50	50	Bulging	7880	5163						
A33	HSC80-T0.5-V300-M1.0-Fc20	20	300	Perforation	21900			20057			
A34	HSC80-T0.5-V300-M1.0-Fc25	25		Perforation	21900			20066			
A35	HSC80-T0.5-V300-M1.0-Fc30	30		Perforation	21900	20121					
A36	HSC80-T0.5-V300-M1.0-Fc35	35		Perforation	21900	20183					
A37	HSC80-T0.5-V300-M1.0-Fc40	40		Perforation	21900	20238					
A38	HSC80-T0.5-V300-M1.0-Fc50	50		Perforation	21900	20334					

Figure 4 visually presents the relationship between V_m and E_c due to local damage, featuring a regression curve. The regression curve can be appropriately characterized by a quadratic curve that passes through the origin. This configuration ensures that E_c due to local damage is zero when the V_m is zero, resembling scenarios of static loading. This representation strongly aligns with the analysis results. This correlation encompasses both the simulation of impact test results outlined in Table 1 and the supplementary analysis findings outlined in Table 3, which were aimed at extrapolating beyond the ranges of the initial impact test cases.

The differences in E_c tend to diminish as the panel thickness increases. These discrepancies in E_c across various panel thicknesses arise from variations in the efficiency of energy transformation, which transfers kinetic energy from the missile to the internal energy absorbed by the crushed concrete. In accordance with the law of conservation of momentum, the kinetic energy contributing to the local damage of the concrete is determined by subtracting the effect of rigid body velocity of the overall concrete panel from the initial kinetic energy of the missile. This rigid body velocity is higher for panels with thinner thicknesses. For actual structures subject to missile impact, this kinematic energy of the overall panel is transferred to the internal energy due to the global deformation of the panel. In the pursuit of establishing local failure criteria for HSCs, this study adopts the approach of eliminating the influence of energy absorbed by global failure. This is achieved by assuming an infinitely supportive span, thereby focusing solely on the local failure mechanisms in the analysis.

The relationship between M_m and E_c , resulting from local damage in the crushed concrete, is visually presented in Figure 5, which features a regression line. The regression line shows that E_c , attributable to local damage in the crushed concrete, increases proportionally with M_m when V_m is constant. This configuration ensures that E_c , due to local damage of concrete, is zero when V_m is zero.

The strain rate effect of concrete, as applied in the analyses, is shown in Figure 6, as proposed by Malvar et al. (1998). The rate enhancement of concrete tends to be greater with lower f_c' . The relationship between f_c' and E_c , due to local damage in the crushed concrete, is visually presented in Figure 7. The variation in E_c , as evaluated by the analyses, is negligible for various f_c' when the other impact parameters remain constant.

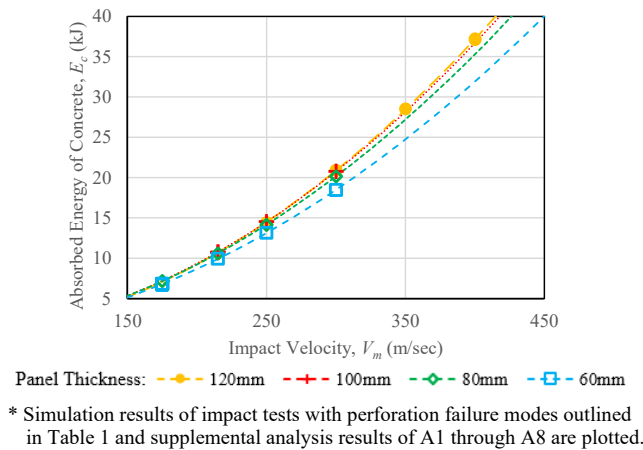


Figure 4. Relationship between V_m and E_c

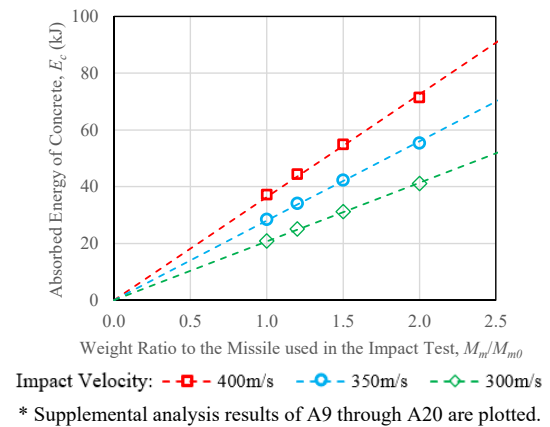


Figure 5. Relationship between M_m and E_c

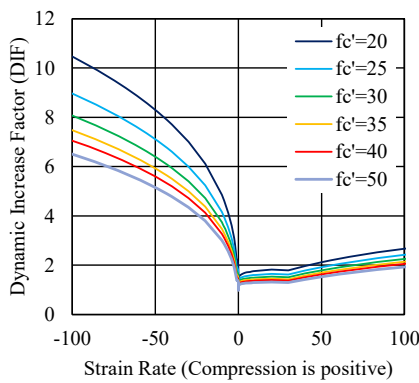


Figure 6. Strain rate effect

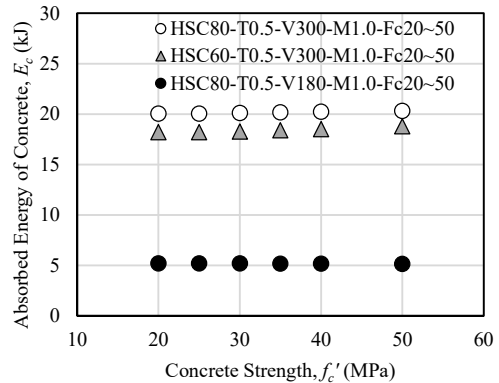


Figure 7. Relationship between f_c' and E_c

According to the relationship between E_c , V_m , M_m and f_c , the expected E_c can be expressed by Equation 1.

$$E_c = \frac{M_m(A \cdot V_m^2 + B \cdot V_m)}{M_{m0}} \quad (1)$$

Where, A and B are factors that express the relationship between E_c and V_m . A= 0.2335 and B=-0.4148 for less momentum of the overall panel after missile impact.

PROPOSAL OF FAILURE CRITERIA

Based on the expected E_c obtained according to Equation 1, the energy demand required to be absorbed by steel plate, can be calculated by subtracting E_c from the kinematic energy of the impact missile, $K_m=0.5M_mV_m^2$. E_s can be theoretically calculated using Equation 2, based on the assumption shown in Figure 8. The analytical results depicted in Table 2 show that the plastic strain distribution is concentric and the gradient of plastic strain is almost constant, as illustrated in Figure 8 (b). The stress – strain relationship is assumed to be rigid-plastic for simplification, as shown Figure 8 (c). The triaxial factor (TF=2) is considered for the strain at fracture.

$$E_s = \int_0^{2\pi} \int_0^R \varepsilon_{cr}(1 - r/R) \cdot \left[\frac{(\sigma_y - \sigma_u)r}{R} + \sigma_u \right] \cdot T \cdot r \cdot dr \cdot d\theta \quad (2)$$

$$= 1/6 \pi \cdot (\sigma_u + \sigma_y) \cdot \varepsilon_{cr} \cdot T \cdot R^2, \quad R = t + b/2$$

Where, E_s is theoretical energy absorption capacity of steel plate, b is diameter of missile, T is thickness of steel plate, σ_y and σ_u are yield and maximum strength of steel plate, ε_{cr} is fracture strain of steel plate considering triaxial factor. The other parameters are based on Figure 8.

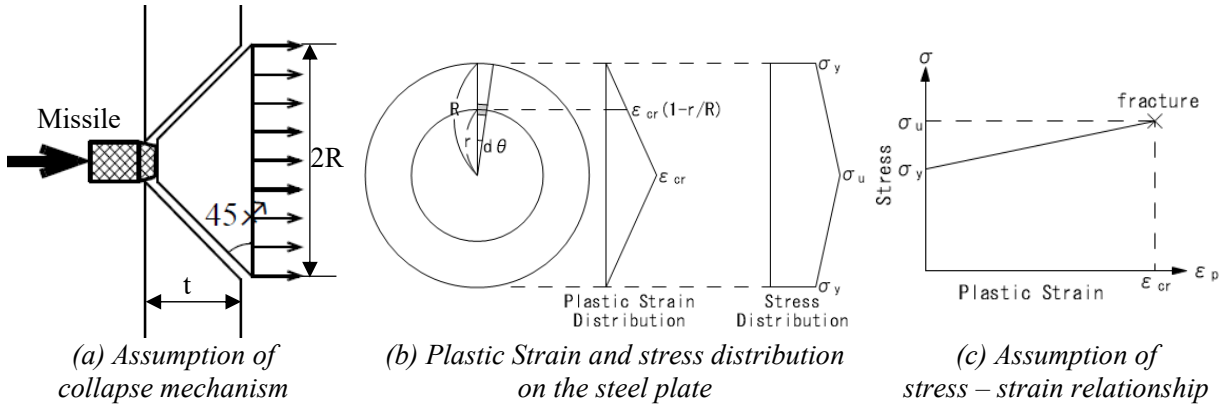


Figure 8. Assumption on calculation of energy absorption capacity of steel plate

The perforation criteria of HSC are expressed as follows.

$$(K_m - E_c) / E_s < 1.0 \quad (3)$$

Where, K_m is kinematic energy of the missile $K_m=0.5M_mV_m^2$. According to Equations 1 to 3, required thickness of the steel plate is explicitly expressed as follows under the condition where the momentum of overall panel after missile impact is negligible.

$$T > \frac{3\{0.486M_mV_m^2 - 2M_m(0.2335V_m^2 - 0.4148V_m)\}}{0.486\pi(\sigma_u + \sigma_y) \cdot \varepsilon_{cr} \cdot (t + b/2)^2} \quad (4)$$

VERIFICATION OF FAILURE CRITERIA

The verification analyses, as outlined in Table 4, were conducted to assess the accuracy of the perforation criteria outlined in Equation 4. These analyses involved models with thicker HSC panels (200mm and 300mm) subjected to more substantial missile impacts, as shown in Figure 9. Additionally, they included models that resemble the simulation of impact tests with varying thicknesses (60mm through 120mm), as shown in Figure 2. The modelling approach, including material models and mesh size, applied to the thicker analysis models, remained consistent with those validated through the simulation of impact tests.

Table 4: Verification analysis results to establish relationship between impact parameters and E_c

Verification Analysis Case		Impact Parameters				Impact Analysis Results				
		Concrete Strength f_c' (MPa)	Missile Weight Multiplier M_m / M_{m0}	Panel Thickness t (mm)	Steel Plate Thickness T (mm)	Target Velocity V_m (m/sec)	Failure Mode	Initial Kinematic Energy of Missile K_m (J)	Absorbed Energy by Concrete E_c (J)	
No.	Label									
V1	HSC60-T1.2-V175-M1.0-Fc30	30	1.0	60	1.2	175	Bulging	7446	6751	
V2	HSC60-T1.6-V175-M1.0-Fc30				1.6	175	Bulging	7446	6729	
V3	HSC60-T1.2-V215-M1.0-Fc30				1.2	215	Perforation	11240	9926	
V4	HSC60-T1.6-V215-M1.0-Fc30				1.6	215	Perforation	11240	9931	
V5	HSC60-T2.4-V215-M1.0-Fc30				2.4	215	Bulging	11240	9931	
V6	HSC60-T3.2-V215-M1.0-Fc30				3.2	215	Bulging	11240	10012	
V7	HSC80-T1.6-V250-M1.0-Fc30			80	1.6	250	Bulging	15200	14120	
V8	HSC100-T0.8-V300-M1.0-Fc30			100	0.8	300	Bulging	21900	20753	
V9	HSC100-T1.2-V300-M1.0-Fc30				1.2	300	Bulging	21900	20828	
V10	HSC120-T0.8-V350-M1.0-Fc30			120	0.8	350	Bulging	29800	28452	
V11	HSC120-T1.2-V350-M1.0-Fc30		1.2		350	Bulging	29800	28464		
V12	HSC120-T0.8-V400-M1.0-Fc30		0.8		400	Bulging	38900	37075		
V13	HSC120-T1.4-V400-M1.0-Fc30		1.4		400	Bulging	38900	36999		
V14	HSC200-T0.5-V200-M10-Fc30		10	200	0.5	200	Perforation	97250	91343	
V15	HSC200-T0.8-V200-M10-Fc30				0.8	200	Splitting	97250	91227	
V16	HSC200-T1.2-V200-M10-Fc30				1.2	200	Bulging	97250	91090	
V17	HSC200-T1.2-V250-M10-Fc30				1.2	250	Perforation	152000	141391	
V18	HSC200-T1.6-V250-M10-Fc30			1.6	250	Bulging	152000	141281		
V19	HSC200-T2.4-V250-M10-Fc30			2.4	250	Bulging	152000	141141		
V20	HSC300-T1.2-V300-M20-Fc30			20	300	1.2	300	Perforation	437600	410797
V21	HSC300-T1.6-V300-M20-Fc30					1.6	300	Bulging	437600	410624
V22	HSC300-T2.4-V300-M20-Fc30		2.4			300	Bulging	437600	410220	
V23	HSC300-T1.6-V350-M20-Fc30		1.6		350	Perforation	595700	559182		
V24	HSC300-T2.4-V350-M20-Fc30		2.4		350	Bulging	595700	559080		
V25	HSC300-T3.0-V350-M20-Fc30		3.0	350	Bulging	595700	559124			

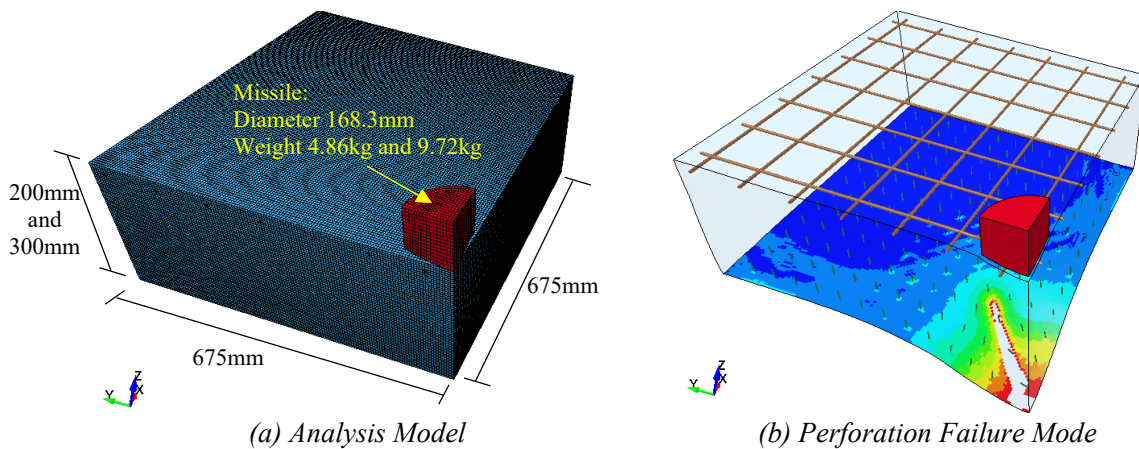


Figure 9. Supplementary analysis for validation of perforation criteria of HSCs

Table 5 summarizes the failure modes of all the verification analysis cases outlined in Table 4. These encompass the scenarios outlined in Table 1, which simulate the impact tests, and a part of supplementary analysis cases detailed in Table 3 which were crucial in developing the perforation criteria denoted by Equation 4. Table 5 also presents the assessment results for the perforation of HSC panels using various methods. These methods include impact tests, the perforation criteria based on Equation 4, and the conventional Chang formula (1981), which treats the HSC panels as RC panels. Table 5 indicates that the inclusion of the steel plate effectively prevents scattered concrete, in line with the proposed criteria expressed in Equation 4. However, the results obtained from Equation 4 for assessing the impact resistance are more conservative than the outcomes of FEM analysis. This discrepancy is particularly noticeable in impact analysis scenarios involving HSC panels with relatively light missile weight, such as those with a thickness of 120mm subjected to a 0.486kg missile impact, for example.

Table 5: Results by various evaluation methods for local failure of HSCs

Test/ Analysis Case No.	Panel Thickness (mm)	Impact Velocity (m/s)	Steel Plate Thickness (mm)	Evaluation Method						
				Impact Test	FEM Analysis	Perforation Criteria for HSC (Equation 4)	Chang Formula for Scabbing (Required Thickness, mm)			
T9	60	140	0.5	Splitting	Splitting	Perforation	NG (68)			
T11			0.5	Perforation	Perforation	Perforation				
T15 & T16		175	0.8	Bulging	Perforation	Perforation	NG (79)			
V1			1.2	—	Bulging	Perforation				
V2			1.6	—	Bulging	Bulging				
T18			0.8	Perforation	Perforation	Perforation				
V3		215	1.2	—	Perforation	Perforation	NG (91)			
V4			1.6	—	Perforation	Perforation				
V5			2.4	—	Bulging	Perforation				
V6			3.2	—	Bulging	Bulging				
T10			80	140	0.5	Bulging		Bulging	Bulging	OK (68)
T12					0.5	Bulging		Bulging	Bulging	
T17	175	0.8		Bulging	Bulging	Bulging	OK (79)			
T22		1.2		Bulging	Bulging	Bulging				
T13		0.5		Perforation	Perforation	Perforation				
T19	215	0.8		Bulging	Bulging	Perforation	NG (91)			
T23		1.2		Bulging	Bulging	Bulging				
T20		0.8		Perforation	Perforation	Perforation				
T24		250		1.2	Splitting	Splitting		Perforation	NG (101)	
V7	1.6			—	Bulging	Bulging				
T14	100	250	0.5	Bulging	Bulging	Perforation	NG (101)			
T21			0.8	Bulging	Bulging	Bulging				
A7		300	0.5	—	Perforation	Perforation	NG (114)			
V8			0.8	—	Bulging	Perforation				
V9			1.2	—	Bulging	Bulging				
A13			0.5	—	Bulging	Perforation				
V10	350	0.8	—	Bulging	Perforation	NG (126)				
V11		1.2	—	Bulging	Bulging					
A17		0.5	—	Perforation	Perforation					
V12	400	0.8	—	Bulging	Perforation	NG (138)				
V13		1.4	—	Bulging	Bulging					
V14		0.5	—	Perforation	Perforation					
V15	200*	200	0.8	—	Splitting	Perforation	NG (286)			
V16			1.2	—	Bulging	Bulging				
V17			1.2	—	Perforation	Perforation				
V18		250	1.6	—	Bulging	Bulging	NG (332)			
V19			2.4	—	Bulging	Bulging				
V20			1.2	—	Perforation	Perforation				
V21	300*	300	1.6	—	Bulging	Perforation	NG (375)			
V22			2.4	—	Bulging	Bulging				
V23			1.6	—	Perforation	Perforation				
V24		350	2.4	—	Bulging	Perforation	NG (416)			
V25			3.0	—	Bulging	Bulging				

* The dimensions of Missile and HSCs are shown in Figure 9. Those for the other analysis cases are based on Figure 2.

The FEM analysis can simulate the rebound of the missile after impact, especially when the weight of the missile is relatively lighter than that of the HSC. This capability allows for the consideration of the efficiency of energy transformation from the initial kinetic energy of the relatively light missile into the internal energy of the HSCs. This transformation is associated with the damage of concrete and the steel plate. Consequently, the assessment results from Equation 4, based on impact conditions where the momentum of the overall panel and the missile after impact is less, become more conservative than the FEM analysis results when the momentum of the overall panel or the missile after impact is significant.

CONCLUSION

The effects of impact parameters, including impact velocity (V_m), missile weight (M_m), panel thickness (t), and concrete strength (f_c'), on the energy absorption mechanism against missile impact – specifically, the energy absorbed by the local damage of the concrete (E_c) – were explored through supplementary analyses conducted alongside the original impact test cases. By examining the relationship between the expected E_c and various impact parameters investigated in the impact analyses, and considering the theoretical energy absorption capacity of the steel plate, the perforation criteria for HSC were developed. The proposed formula proves useful in design by determining the optimal steel plate thickness (T) and concrete panel thickness (t) to prevent both scattered concrete and missile perforation. This determination is made based on impact parameters such as impact velocity (V_m), missile weight (M_m), and missile diameter (b), eliminating the need for extensive FEM analysis.

Based on the comparison of assessment results, treating the HSC panels as RC panels to apply the conventional formula was overly conservative. The assessment results, based on the proposed perforation criteria for HSCs, showed a slight conservatism compared to the FEM analysis results, especially for the impact analysis cases with relatively light-weight missiles compared to that of the HSC. Since the FEM analysis can demonstrate the rebound of the missile after impact, it considers the efficiency of energy transformation from the initial kinetic energy of the missile to the internal energy of the HSCs. Further studies exploring the efficiency of energy transformation from the missile's kinetic energy to the internal energy of damaged concrete and steel plate, while considering the principles of conservation of momentum and the flexibility of the missile, could mitigate the inherent conservativeness in the proposed formula.

REFERENCES

- Hashimoto J., Takiguchi K., Nishimura K., Matsuzawa K., Tsutsui M., Ohashi Y., Kojima I. and Torita H. (2005). “Experimental Study on Behavior of RC Panels Covered with Steel Plates Subjected to Missile Impact,” *18th SMiRT*, J05-4.
- Tsukada T., Kuramoto S., and Ohashi Y. (2022). “Analytical Study on Behavior of RC Panels Covered with Steel Plate Subject to Missile Impact,” *26th SMiRT*, We.2.B.1.
- Chang W. S. (1981), “Impact of Solid Missile on Concrete Barriers”, *Journal of the Structural Division*, ASCE, Vol.107, No.ST2, pp.257-271.
- National Defense Research Committee (1946), “Effects of Impact and Explosion”, *Summary Technical Report of Division 2*, Vol.1, Washington DC.
- Degen P. (1980), “Perforation of Reinforced Concrete Slabs by Rigid Missiles”, *Journal of the Structural Division*, ASCE, Vol.106, No.ST7, pp.1623-1642.
- Crawford et al. (2011). “Use and Verification of the Release III K&C Concrete Material Model in LS-DYNA” *Karagozian & Case*.
- Comité Euro-International du Béton (2013). “fib Model Code for Concrete Structures 2010” *Ernst & Sohn Verlag*.
- Malvar L. J. and Crawford J. E. (1998). “Dynamic Increase Factors for Concrete” *28th DDESB Seminar at Orlando*.